

Supplemental Materials

Combinatorial Release of Dexamethasone and Amiodarone From a Nano-structured Parylene-C Film to Reduce Perioperative Inflammation and Atrial Fibrillation

Erik Robinson, PhD,^{1, *, ‡} Sunjay Kaushal, MD,^{2, *, §} Justice Alaboson, PhD,³ Sudhish Sharma, PhD,⁴ Amogh Belagodu, MS,⁵ Claire Watkins, MD,⁴ Brandon Walker, MSc,⁴ Gregory Webster, MD,⁶ Patrick McCarthy, MD,^{7, §} Dean Ho, PhD^{1, 8, 9, ¥, †, §}

¹Department of Mechanical Engineering, Northwestern University, Evanston, Illinois, 60208

²Division of Pediatric Cardiac Surgery, University of Maryland School of Medicine, Baltimore, MD, 21201

³Department of Material Science and Engineering, Northwestern University, Evanston, Illinois, 60208

⁴Ann and Robert H. Lurie Children's Hospital of Chicago, Chicago, IL, 60611

⁵Department of Chemical & Biological Engineering, Northwestern University, Evanston, Illinois, 60208

⁶Division of Cardiology, Ann and Robert H. Lurie Children's Hospital of Chicago, Northwestern University, Feinberg School of Medicine, Chicago, IL, 60611

⁷Division of Cardiac Surgery, the Bluhm Cardiovascular Institute, Northwestern University Feinberg School of Medicine, Chicago, IL, 60611

⁸Department of Biomedical Engineering, Northwestern University, Evanston, Illinois, 60208

⁹Robert H Lurie Comprehensive Cancer Center, Northwestern University, Chicago, Illinois, 60611

[‡]Current Address & Affiliation: Sintact Medical Systems, Inc., 113 E. 6th St., Bloomington, IN, 47408

[¥]Current Address: Division of Oral Biology and Medicine, Division of Advanced Prosthodontics, and The Jane and Jerry Weintraub Center for Reconstructive Biotechnology, UCLA School of Dentistry, Los Angeles, California, 90095

†Current Affiliations: Department of Bioengineering, California NanoSystems Institute and Jonsson Comprehensive Cancer Center, UCLA, Los Angeles, California, 90095

*These authors contributed equally to this work

§To whom correspondence should be addressed: erik@sintactmed.com, dean.ho@ucla.edu, skaushal@smail.umaryland.edu, pmccart@nmh.org

Keywords: Adhesion, Inflammation, Wound Healing, Drug Delivery, Controlled Drug Release, Heart

Word Count: 1,647

Erik Robinson, PhD

Chief Executive Officer

Sintact Medical Systems

113 E. 6th St.

Bloomington, IN 47408

Phone: (312) 493-3140

Email: erik@sintactmed.com

Dean Ho, PhD

Professor and Co-Director

The Jane and Jerry Weintraub Center for Reconstructive Biotechnology

Division of Oral Biology and Medicine

Department of Bioengineering

10833 Le Conte Avenue

B3-068A

Los Angeles, CA 90095-1668

Phone: (310) 794-9851

Email: dean.ho@ucla.edu

Sunjay Kaushal, M.D., Ph.D.

Associate Professor

Division of Cardiac Surgery

Director of Pediatric Cardiac Surgery

University of Maryland Medical Center

110 S. Paca Street, 7th floor

Baltimore, MD 21201

Phone: (410) 328-5842

Fax: (410) 328-2750

Pager: (410) 850-8429

Cell Phone (443)-826-0206

Patrick M. McCarthy, M.D.

Chief, Division of Cardiac Surgery

Director, Bluhm Cardiovascular Institute

Heller-Sacks Professor of Surgery

Northwestern University Feinberg School of Medicine

201 East Huron Street, Galter 11-140

Chicago, IL 60611-2968

Phone: 312.695.3114

Fax: 312.695.0178

pmccart@nmh.org

Materials and Methods

Material Fabrication

20 grams of Parylene-C (dichloro(2,2)paracyclophane) (PPX) (Paratech Coating Inc., Aliso Viejo, CA) was deposited onto various substrates. Deposition occurred within a Labcoter 2 PDS 2010 (Specialty Coating Systems SCS, Indianapolis, IN) under default conditions.(1) Drug loading involved applying 150 µg of DEX (Alfa Aesar, Ward Hill, MA) and 800 µg of AMIO (U.S. Pharmacopeia, Rockville, MD) on PPX surfaces (600 µg of DEX and 3.2 mg of AMIO total), which was then repeated. Deposition of sub-conformal PPX layer was over each layer of drug followed by plasma oxidation of the surface with a PDC-001 expanded plasma cleaner coupled with a PlasmaFlo gas mixer (Harrick Plasma, Ithaca, NY). This process was not applied to the superficial most layer of PPX – this layer was left hydrophobic, compared to PPX-Oxd which was oxidized and remained hydrophilic. Sterilization of drug loaded films occurred through exposure to ethylene oxide gas utilizing an Anprolene AN74i gas sterilizer (Anderson Products, Inc. Haw River, NC) per manufacturer's recommendations.

In vitro Analysis

In-vitro analysis and drug release was completed through deposition of PPX on varying culture plates. Surface treatment of PPX culture plates consisted of plasma oxidation (Oxd) or lack thereof resulting in hydrophilic or hydrophobic surfaces (native form). RAW264.7 macrophages and NIH-3T3 fibroblasts were analyzed on varying surfaces to determine *in-vitro* response. Cells were kept in DMEM media supplemented with 10% FBS and 1% Pen/Strep in humidified atmosphere with 5% CO². Cellular analysis was completed through the application of time lapse bright field imaging in addition to multiple cellular assays examining viability (MTT, Roche Diagnostics), proliferation (CyQUANT, Life Technologies), and adhesion (Vybrant, Molecular Probes) onto polystyrene, representing baseline biocompatible control surfaces, and various PPX surfaces. RNA isolation was accomplished utilizing TRIzol reagent (Invitrogen Corporation, Carlsbad, CA) per the manufacturer's guidelines. cDNA was synthesized using the

iScript Select cDNA Synthesis Kit (Quanta Biosciences, Gaithersburg, MD). qRT-PCR was done using SYBER Green detection reagents (Quanta Biosciences, Gaithersburg, MD) and appropriate primers for IL-6 and β -Actin (Integrated DNA Technologies, Coralville, IA). Samples were amplified using a MyiQ real-time PCR detection system (Bio-Rad).

Material Characterization

X-ray Photoelectron Spectroscopy (XPS) was completed using an Omicron ESCA probe (Omicron NanoTechnology, Eden Prairie, MN) coupled with an EA125 hemispherical energy analyzer. Photoemission was stimulated through monochromated Al (KR) radiation (1486.6 eV) with a power output of 300 W under ultra-high vacuum (UHV). Survey scans completed by the analyzer were maintained in constant analyzer energy (CAE) mode at 50 eV. Binding energies were referenced at the C 1s (285.0 eV) binding energy set. The binding energy spectrum for each XPS survey scan ranged from 0 – 1200 eV. Surface wettability was determined through static contact angle measurements using a VCA Optima contact angle goniometer (AST Products, Inc., Billerica, MA) equipped with an automated pipetting system. Ultrapure H₂O volumes of 15 μ l were dispensed on varying substrates and subsequent images and angle measurements were collected through AutoFAST Imaging and SPC software respectively. Atomic Force Microscopy (AFM) images were collected utilizing a CP Research (Formally ThermoMicroscopes now Veeco Instruments Inc., Plainview NY) AFM. Imaging was performed in intermittent contact mode using a Si probe, (μ Masch, NSC36A) with a nominal tip radius curvature of 10 nm. AFM images were rendered and analyzed using WSXM SPM analysis software.(2) Profile measurements concerning film thickness were completed utilizing a Veeco Dektak 150 Surface Profiler (Veeco Instruments Inc., Plainview, NY) using a standard scan option equipped with a 2.5 μ m stylus with an applied force of 5.0 mg. Scan length and duration were confined between 1500 – 2000 μ m and 90 seconds respectively, resulting in horizontal resolutions of 0.055 μ m to 0.075 μ m and vertical resolution maximum of 524 μ m. Analysis was completed using Dektak V9 Software. Attenuated total reflection (ATR) Fourier transform

infrared (FT-IR) spectroscopy was performed utilizing a Thermo Nicolet Nexus 870 IR Spectrophotometer (ThermoFisher Scientific Inc., Waltham, MA). FT-IR analyses of the films under investigation were loaded onto an attenuated reflectance kit (ARK) with a Zinc Selenium (ZnSe) crystal contained within a N₂ purged chamber. A liquid nitrogen cooled mercury cadmium telluride (MCT) detector completed 64 scans with a resolution of 8 cm⁻¹ over a range of 4,000 – 650 cm⁻¹ at room temperature. Samples were loaded onto the ZnSe crystal at a point to point contact interface under maximum allowable load/pressure. ATR and further baseline corrections were completed utilizing Omnic and eFTIR software. All measurements were completed in air and under ambient conditions unless stated otherwise.

Animal Preparation

This work was approved by the Children's Memorial Research Center and the University Of Maryland School Of Medicine's Institutional Animal Care and Use Committee. Thirty New Zealand white female rabbits (4 kg) were randomly assigned to one of five groups: Control group (N=6), oxidized PPX (PPX-Oxd, N=6), PPX-Oxd infused with DEX (PPX-Oxd[DEX], N=6), native PPX (PPX, N=4), and PPX infused with DEX and AMIO (PPX[AMIO, DEX], N=6). Initial sedation with acepromazine (0.5 mg/kg subcutaneous) was followed by general anesthesia induction using ketamine (40 mg/kg) and xylazine (7 mg/kg). Endotracheal intubation was achieved with a 3- or 4-mm tube and anesthesia was maintained intraoperatively with 1.5 - 2.5% isoflurane. An intravenous catheter was placed in the marginal ear vein. Cardiorespiratory monitoring was maintained throughout surgery.

Rabbit pericardiotomy model

Following clipping of the fur at the operative site, the skin was prepped with betadine. Approach through a midline sternotomy allowed complete anterior pericardiotomy to be made between the left and right phrenic nerves. To incite microvascular bleeding and pericardial adhesion formation, a gauze pad was used to abrade the epicardial surface of the pericardium for 5 minutes. Experimental biologic membranes were fixed to the edges of the pericardium

using four 5.0 polypropylene sutures as performed in a previous study.(3) Control animals had 4 sutures placed in the open pericardium but no membrane. Tube thoracostomy was employed during closure of the sternotomy and subsequently removed.

Arrhythmia induction and measurement

Defibrillation patches were placed on the lateral aspect of the thorax to provide defibrillation if required and to produce a single-lead surface electrocardiogram. The electrocardiogram was recorded using a Medtronic LIFEPAK® 20/20e Defibrillator/ Monitor. The atrium was identified by morphology and contraction sequence. Bipolar atrial wires were affixed (Medtronic temporary myocardial pacing wires, model number 6494). A bipolar electrogram was used to confirm placement, if needed. A surface electrogram was generated at a paper speed of 25 mm/sec and the atrium was exposed to an International Electrotechnical Commission 6LR61 alkaline battery to produce atrial fibrillation. Atrial fibrillation was confirmed on the surface electrogram, characterized as high-frequency, low-amplitude atrial electrograms, typically with varying R-R intervals. Because not every exposure to current induced atrial fibrillation, duration of exposure was measured for each attempt, measured as the number of seconds during which the atrial bipolar wires were exposed to the induction current. For each successful induction, atrial fibrillation duration was measured as the number of seconds after the end of induction while the atrium remained in fibrillation.

Cardiac adhesion assessment

Four weeks following pericardial abrasion and treatment, rabbits again underwent anesthesia and repeat sternotomy for the assessment of cardiac adhesion formation. Retrosternal scar tissue was observed by a blinded analyst (Carl Backer, M.D.) and adhesion density at the apex, middle and base of the central epicardium was scored. The gross evaluation was evaluated with a 4 point scoring system (0-3). The scoring system indicated the following degree of adhesions 0: No Adhesions, 1: Mild Adhesions (easily dissected), 2: Moderate Adhesions, and 3: Severe Adhesions (difficult to dissect). Right ventricular epicardial

tissue samples were fixed in 10% formalin, paraffin embedded, and hematoxylin-eosin stained for microscopic evaluation of NTF and adhesion formation. Thickness of NTF, as seen with Masson trichome staining, was observed by a blinded analyst with the National Institutes of Health Image program (version 1.62; National Institutes of Health, Springfield, VA) to measure cardiac adhesion thickness.

Statistical Methods

All data are presented as mean \pm standard deviation. Normally-distributed data are compared by Student *t* test to analyze variance. Data that were not normally distributed were analyzed via Wilcoxon rank-sum test. A *p* value of less than 0.05 was considered significant. The primary outcome measure for arrhythmia was duration of atrial fibrillation per successful induction attempt. In addition, the number of attempts required to put rabbits into atrial fibrillation and duration of exposure to induction current were tabulated. Data analysis and visualization was aided by Daniel's XL Toolbox add-in for Excel, version 6.60, by Daniel Kraus, Wurzburg, Germany (www.xltoolbox.net).⁽⁴⁾

Results

Characterization of PPX Films

AFM images, shown in Figure S1C depict surface features and compositional uniformity among the substrates examined. Visualization of phase images, portions A & C, in Figure S1C, reveal surfaces composed of uniform material, which was an expected result with the polymers under investigation. Images in B & D in Figure S1C show topographical output as a measure of elevation changes across the films. This information was analyzed and interpreted previously in Figure 3D as RMS roughness across each surface.

Chemical analysis of the PPX films was measured through XPS (Figure S2A-E). PPX surface modification (PPX-Oxd) (Figure S2C) shows the impact of plasma oxidation on oxygen content from native PPX (Figure S2B). Compared to the elemental content of control surfaces,

considered biocompatible (Figure S2A), modified PPX (PPX-Oxd) surfaces exhibited similar carbon to oxygen ratios. The Repel™ film (Figure S2D) displayed a varying ratio of carbon to oxygen content, whereby oxygen surpassed the carbon present. In contrast, the Preclude™ (Figure S2E) membrane consisted of fluorine with traces of carbon.

Figure S2F-J depicts FT-IR analysis revealing chemical groups present on each of the film surfaces. Examination of results obtained depict subtle changes to PPX modified films (PPX-Oxd) (Figure S2H) when compared to native PPX (Figure S2G) surfaces. Previous reports indicate the formation of carbonyl C=O groups due to plasma oxidation of the PPX surface which are responsible for the changes to chemical composition(5, 6) as well as cell/tissue response.(7) Repel™ and Preclude™ readouts correspond to their chemical composition shown Figure S2I-J.

Supplementary Figures

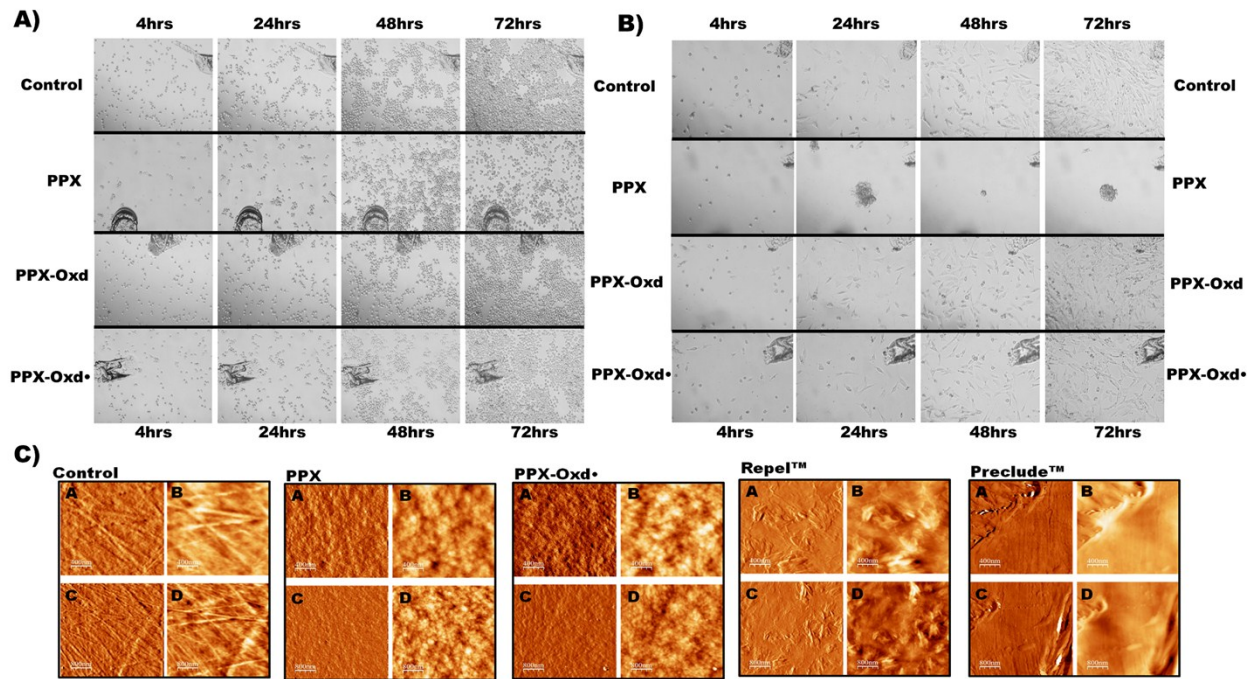


Figure S1: Time lapse images of RAW264.7 murine macrophages A) and 3T3-NIH murine fibroblasts B) grown on varying substrate surfaces over the course of 72 hrs (images taken at corresponding time points 4, 24, 48 and 72 hrs). As indicated by the Control surface RAW264.7 macrophages display comparative monolayer outgrowth on either of the oxidized PPX surfaces (PPX-Oxd, PPX-Oxd•). A somewhat irregular growth pattern is seen on PPX surfaces which did not undergo plasma oxidation. Compared to the Control surface 3T3-NIH fibroblasts display comparative monolayer outgrowth on either of the oxidized PPX surfaces (PPX-Oxd, PPX-Oxd•). Striking irregular growth patterns are evident on PPX surfaces which did not undergo plasma oxidation, leading to the assertion the fibroblasts were unable to adhere to the PPX surface. Atomic Force Microscopy (AFM) images C) of surfaces (Control, PPX and PPX-Oxd) and films (Repel™ and Preclude™) under investigation. Image sets denoted by A & C reveal phase images compared to topographical outputs on B & D. Phase images reveal similar material properties across the surface. Uniform shading indicates the surface is composed of a

similar material. Topographical images reflect changes in elevation across the film surface. Alterations in shading correspond to depressions or elevations across the film surface. Images A & B and C & D represent zoom in and zoom out functions respectively.

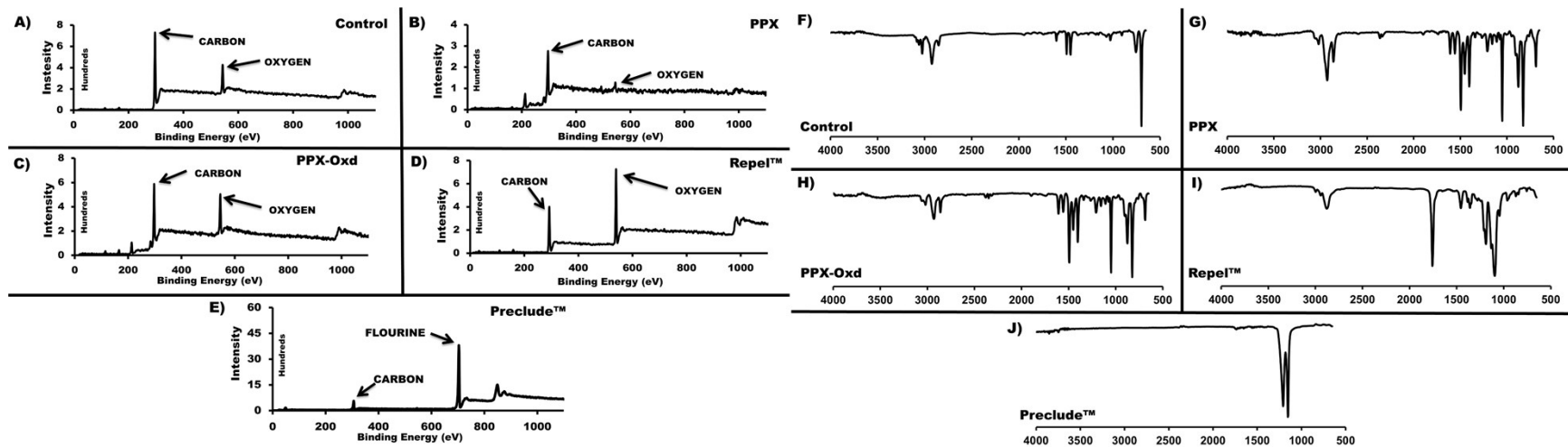


Figure S2: X-Ray Photoelectron Spectroscopy (XPS) measurements identifying constituent elements present on substrate surfaces. Elemental analysis revealed varying carbon and oxygen ratios as the primary elemental composition on each of the films, excluding the Preclude™ membrane. Control surfaces (A) revealed a greater degree of carbon to oxygen content. Comparatively, PPX (B) showed a decrease in oxygen content when compared to carbon. Oxidized PPX (C) (PPX-Oxd) reveals an increase in oxygen which can be attributed to the oxygen plasma surface bombardment. It is of interest to note, the carbon/oxygen balance similarities between Control and PPX-Oxd substrates. The Repel™ (D) film is the only surface present whose oxygen content supersedes the amount of carbon present. Preclude™ (E) remaining the striking exception, as it contains a predominate amount of fluorine on the surface with negligible carbon content. FT-IR surface scans representing chemical species present on the surface of the respective films. F) Control surfaces, consisting of plasma oxidized polystyrene compared to various PPX conditions. G) Native PPX surface

and H) oxidized PPX (PPX-Oxd) appear quite similar attributing changes to a weak carbonyl C=O signal between the transmission spectra. Repel™ I) and Preclude™ J) spectra are provided for comparison of current clinical anti-adhesive barriers.

References

1. Boduroglu S, Cetinkaya M, Dressick WJ, Singh A, Demirel MC. Controlling the Wettability and Adhesion of Nanostructured Poly-(p-xylylene) Films. *Langmuir*. 2007;23(23):11391-5.
2. Horcas I, Fernandez R, Gomez-Rodriguez JM, Colchero J, Gomez-Herrero J, Baro AM. WSXM: A software for scanning probe microscopy and a tool for nanotechnology. *Review of Scientific Instruments*. 2007;78(1).
3. Kaushal S, Patel SK, Goh S-K, Sood A, Walker BL, Backer CL. A novel combination of bioresorbable polymeric film and expanded polytetrafluoroethylene provides a protective barrier and reduces adhesions. *Journal of Thoracic and Cardiovascular Surgery*. 2011;141(3):789-95.
4. Kraus D. Consolidated data analysis and presentation using an open-source add-in for the Microsoft Excel® spreadsheet software. *Medical Writing*. 2014;23(1):25-8.
5. Kahouli A, Sylvestre A, Laithier JF, Pairis S, Garden JL, Andre E, et al. Effect of O-2, Ar/H-2 and CF4 plasma treatments on the structural and dielectric properties of parylene-C thin films. *Journal of Physics D-Applied Physics*. 2012;45(21).
6. Lee JH, Hwang KS, Kim TS, Seong JW, Yoon KH, Ahn SY. Effect of oxygen plasma treatment on adhesion improvement of Au deposited on Pa-c substrates. *Journal of the Korean Physical Society*. 2004;44(5):1177-81.
7. Song JS, Lee S, Jung SH, Cha GC, Mun MS. Improved biocompatibility of parylene-C films prepared by chemical vapor deposition and the subsequent plasma treatment. *Journal of Applied Polymer Science*. 2009;112(6):3677-85.